J. Fluid Mech. (2007), *vol.* 589, *pp.* 305–314.
doi:10.1017/S0022112007008178 Printed in the United Kingdom

Gas flows in microchannels and microtubes

CHUNPEI CAI[1], QUANHUA SUN[2] AND IAIN D. BOYD[3]

[1]ZONA Technology Inc., Scottsdale, AZ 85258, USA

[2]ESI US R&D, Huntsville, Alabama 35806

[3]Department of Aerospace Engineering, University of Michigan, Ann Arbor, MI 48109, USA

(Received 15 February 2007 and in revised form 3 August 2007)

This study analyses compressible gas flows through microchannels or microtubes, and develops two complete sets of asymptotic solutions. It is a natural extension of the previous work by Arkilic *et al.* on compressible flows through microchannels. First, by comparing the magnitudes of different forces in the compressible gas flow, we obtain proper estimations for the Reynolds and Mach numbers at the outlets. Second, based on these estimations, we obtain asymptotic analytical solutions of velocities, pressure and temperature distributions of compressible gas flow inside the microchannels and microtubes with a relaxation of the isothermal assumption, which was previously used in many studies. Numerical simulations of compressible flows through a microchannel and a microtube are performed by solving the compressible Navier–Stokes equations, with velocity slip and temperature jump wall boundary conditions. The numerical simulation results validate the analytical results from this study.

1. Introduction

Microchannels are important components for many micro-electro-mechanical systems (MEMS), and they are used to transport gas in many MEMS devices. In the literature, there are many discussions about gas flows in tubes (see for example Prud'homme, Champman & Brown 1986; van den Berg, ten Seldam & van der Guli 1993; Harley & Huang 1995). It is found that because of the small scale microchannel flows exhibit many interesting phenomena that were not observed in their large-scale counterparts. For example, the experimental measurements by Pong, Ho & Liu (1994) and Arkilic, Schmidt & Breuer (1997) showed that the gas pressure distribution along a microchannel is not linear, and there is obvious velocity slip on the channel wall. It is well accepted that for microchannel flows the Navier–Stokes equations are still applicable if a slip wall boundary condition is used. Several analytical solutions for the flow field have been presented using the isothermal assumption, for example, the work by Arkilic, Schmidt & Breuer (2001) and Zohar *et al.* (2004). More complicated results have also been obtained numerically using kinetic-based approaches, including the direct simulation Monte Carlo method by Ho & Tai (1998) and Zheng, Garcia & Alder (2000), the information preservation method by Cai *et al.* (2000) and Shen, Fan & Xie (2003), and the gas-kinetic BGK–Burnett method by Xu & Li (2004).

The work in this paper aims to extend Arkilic *et al.*'s original work to compressible gas flows in microchannels and microtubes by removing the isothermal assumption. In many cases, the isothermal assumption is not valid and a correctly predicted temperature field is required. Large temperature variation may exist in short microchannel flows. For instance, based on figures 6 and 3(*c*) in Xu & Li (2004), the

temperature variation along a channel centreline is found to reach over 20%. The temperature variation will also build up in long channels. Even when the temperature variation is not significant, the temperature gradient can be very important for heat conduction problems, and it may need special attention for maintenance and system integration in a microsystem environment. The small height of microchannels or microtubes will usually result in large temperature gradients, which cannot be predicted using the isothermal assumption. Also, it is difficult to obtain an analytical expression for the temperature field; an ill-posed energy equation is usually obtained using the asymptotic approach. Hence, a study of the temperature field inside a microchannel or a microtube is of practical importance with mathematical significance. Therefore, some recent research work has investigated the temperature field or the heat transfer in microchannels or microtubes, for example, Kedzierski (2003), Wang & Li (2004), Hetstroni *et al.* (2005) and Qin, Sun & Yin (2007).

2. Problem description and governing equations

Microchannel and microtube flows are very similar, but distinguished by the geometry where the former is two-dimensional and the latter is axisymmetric. Here we use microchannel flows as an example to illustrate our analysis, and the same principles are applicable to microtube flows.

Suppose a microchannel has a height of H and a length of L, and the average gas properties of the compressible outflow are: pressure p_o, density ρ_o, temperature T_o, velocity U_o, and number density n_o, where subscript o denotes an average quantity at the outlet. The inlet pressure should be larger than the outlet pressure in order to drive the flow. The temperature is allowed to have small variations, which removes the isothermal condition used by Arkilic *et al.* and Zohar *et al.* The averaged quantities at the outlet are used to normalize the following governing equations and boundary conditions.

The Navier–Stokes equations for steady, compressible gas flows can be written as

$$\frac{\partial(\rho V_i)}{\partial x_i} = 0, \quad \rho V_j \frac{\partial V_i}{\partial x_j} = \frac{\partial \tau'_{ij}}{\partial x_j} - \frac{\partial p}{\partial x_i}, \quad \rho V_i C_p \frac{\partial T}{\partial x_i} = k\frac{\partial^2 T}{\partial x_i^2} + \tau'_{ij}\frac{\partial u_i}{\partial x_j}, \quad p = \rho RT,$$

where $\tau'_{ij} = \mu(\partial u_i/\partial x_j + \partial u_j/\partial x_i) - \frac{2}{3}\mu\delta_{ij}\partial V_k/\partial x_k$. The velocity slip and temperature jump conditions on the wall follow the expressions in Chen (1996):

$$u_w = \frac{2-\sigma_u}{\sigma_u}\lambda\left(\frac{\partial u}{\partial n}\right)_w + \frac{3}{4}\frac{\mu}{\rho T_w}\left(\frac{\partial T}{\partial x}\right)_w, \quad T - T_w = \frac{2-\sigma_T}{\sigma_T}\frac{2\gamma}{Pr(\gamma+1)}\lambda\left(\frac{\partial T}{\partial n}\right)_w,$$

where $\lambda, \sigma_u, \sigma_T, Pr, \gamma$ are mean free path, momentum accommodation coefficient, energy accommodation coefficient, Prandtl number, and specific heat ratio, and subscript w represents wall properties.

3. Order analysis for Reynolds and Mach numbers

Order analysis provides insight into possible simplification of the problem. To do this, a single control volume of the entire microchannel is taken. If the shear stress on the surface is approximated as $\mu u/(H/2)$, then the momentum equation in the X-direction takes the following form:

$$(p_o - p_i)H + \rho_o u_o H(u_o - u_i) + L\mu(u_o/H + u_i/H) \sim 0$$

$(P-1)\epsilon/Ma^2 : \gamma\epsilon : \gamma/Re$	$Re \sim O(\epsilon)$	$Re \sim O(1)$	$Re \sim O(1/\epsilon)$
$Ma \sim O(\epsilon)$	$(P-1)/\epsilon : \gamma\epsilon : \gamma/\epsilon$	$(P-1)/\epsilon : \gamma\epsilon : \epsilon$	$(P-1)/\epsilon : \gamma\epsilon : \gamma\epsilon$
$Ma \sim O(1)$	$(P-1)\epsilon : \gamma\epsilon : \gamma/\epsilon$	$(P-1)\epsilon : \gamma\epsilon : \gamma$	$(P-1)\epsilon : \gamma\epsilon : \gamma\epsilon$
$Ma \sim O(1/\epsilon)$	$(P-1)\epsilon^3 : \gamma\epsilon : \gamma/\epsilon$	$(P-1)\epsilon^3 : \gamma\epsilon : \gamma$	$(P-1)\epsilon^3 : \gamma\epsilon : \gamma\epsilon$

TABLE 1. Order estimations for different Mach number and Reynolds number combinations.

where subscripts i, o represent averaged quantities at the inlet and outlet, respectively. The Reynolds number based on the average properties at the channel exit, $Re = \rho_o u_o H/\mu$, is usually small, say less than 300. The flow is then assumed laminar.

It is further assumed that the outlet velocity is much larger than the inlet velocity, which is reasonable if the pressure ratio of the inlet to the outlet is larger than 1. Then the following relation is obtained:

$$O((P-1)\epsilon Ma^{-2}) - O(\gamma\epsilon) - O(\gamma/Re) \sim 0, \tag{3.1}$$

where $P = p_i/p_o$ is the pressure ratio, $\epsilon = H/L$ is the aspect ratio, and $Ma = u_o/\sqrt{\gamma RT_o}$ is the Mach number based on the average velocity and temperature at the channel exit. To simplify our analysis, we assume that $1 < P < 10 \ll 1/\epsilon$ and $10^{-1} > \epsilon > 10^{-5}$ in this study.

Mathematically, there are four possibilities among the three terms in (3.1): two terms are significantly greater than the other term and hence these two terms balance each other, or all of the three terms share the same order. The four cases are:

(1) The pressure drop term balances with the convection term while the viscous term is smaller. This leads to $(P-1)\epsilon Ma^{-2} \sim \gamma\epsilon$, $\gamma/Re = o(\gamma\epsilon)$, which requires $\gamma Ma^2 \sim (P-1)$ and $1/Re = o(\epsilon)$. This is a case with large Reynolds and Mach numbers. It is not typical for microchannel flows, and it is not considered in this study.

(2) The pressure drop term balances with the viscous term while the convection term is small. This condition leads to $(P-1)\epsilon Ma^{-2} \sim \gamma/Re$, $\gamma\epsilon = o(\gamma/Re)$. It is easy to show that $\gamma Ma^2/Re = O((P-1)\epsilon)$ and $\gamma Ma^2/(P-1) = o(1)$.

(3) The convection term balances with the viscous term, and the pressure drop term is smaller. Obviously, this is not a pressure-driven case and the velocity will decrease along the channel. This is another case we will not consider in this study.

(4) All of the three terms are of the same order: $(P-1)\epsilon Ma^{-2} \sim \gamma\epsilon \sim \gamma/Re$, which means that $\gamma Ma^2 \sim (P-1)$ and $Re \sim 1/\epsilon$. This is also a high Mach number case, and is not considered.

Thus, Case 2 is the only category to be studied in this work. Specifically, two sub-categories are considered, where the Knudsen number is also given using the relation, $Kn = \sqrt{\pi\gamma/2}(Ma/Re)$:

Case 2A: $Ma \sim O(\epsilon^{1/2})$, $\quad Re \sim O(1)$, $\quad Kn \sim O(\epsilon^{1/2})$;

Case 2B: $Ma \sim O(\epsilon)$, $\quad Re \sim O(\epsilon)$, $\quad Kn \sim O(1)$.

We emphasize that the Mach and Reynolds numbers at the outlet are closely related as indicated by the X-momentum equation. Hence it is improper to assume their orders in an arbitrary manner. Table 1 shows the orders of the three terms (pressure drop, viscous term, convection term) for nine different combinations of Reynolds and Mach numbers. Clearly, only three of the nine cases satisfy the X-momentum balance relation: $Re \sim O(\epsilon)$, $Ma \sim O(\epsilon)$; $Re \sim O(1/\epsilon)$, $Ma \sim O(1)$; $Re \sim O(1/\epsilon)$, $Ma \sim O(1/\epsilon)$. Note that the last case falls into category (iii), which is not pressure driven.

4. Asymptotic solutions for flows in a microchannel

Following the steps in Arkilic *et al.*'s original work, we normalize the flow properties by the averaged values at the channel outlet, the X- and Y-coordinates by the channel length, L, and height, H, and use a prime to denote the non-dimensional quantities. We use the following forms for the non-dimensional quantities:

$$u' = u_1 + \epsilon u_2 + \cdots, \quad v' = v_1 + \epsilon v_2 + \cdots, \quad p' = p_1 + \epsilon p_2 + \cdots,$$
$$\rho' = \rho_1 + \epsilon \rho_2 + \cdots, \quad n' = n_1 + \epsilon n_2 + \cdots.$$

For the flow field in a microchannel, the temperature has less variation than the pressure and density. We assume a quasi-isothermal condition $T' = 1 + \epsilon T_2$ for the temperature, which allows us to obtain an analytical expression for the temperature distribution.

The viscosity coefficient, μ, and the heat conductivity coefficient, k, are assumed to be constant since the temperature variation in microchannels is not large. Putting together all the assumptions, we can organize the governing equations according to orders of ϵ, which results in the following simplified equations:

$$v_1 = 0, \quad \frac{\mathrm{d}p_1}{\mathrm{d}y'} = 0, \quad \frac{\epsilon Re}{\gamma Ma^2}\frac{\mathrm{d}p_1}{\mathrm{d}x'} = \frac{\partial^2 u_1}{\partial^2 y'}, \quad \frac{\partial(p_1 u_1)}{\partial x'} + \frac{\partial(p_1 v_2)}{\partial y'} = 0, \tag{4.1}$$

$$\frac{1}{RePr}\frac{\partial^2 T_2}{\partial y'^2} = -\frac{\gamma - 1}{\gamma} u_1 \frac{\mathrm{d}p_1}{\mathrm{d}x'} - \frac{(\gamma - 1)Ma^2}{\epsilon Re}\left(\frac{\partial u_1}{\partial y'}\right)^2 \tag{4.2}$$

The normalized velocity slip and temperature jump boundary conditions on the wall are

$$u'_w = \Theta_u Kn(x')\left(\frac{\partial u'}{\partial n'}\right)_w, \quad 1 + \epsilon T_2 - T'_w = \Theta_T \frac{2\gamma}{Pr(\gamma + 1)} \epsilon Kn(x')\left(\frac{\partial T_2}{\partial n'}\right)_w, \tag{4.3}$$

where $\Theta_u = (2 - \sigma_u)/\sigma_u$, $\Theta_T = (2 - \sigma_T)/\sigma_T$. Note that in the velocity boundary condition, the temperature gradient term is omitted because it is much smaller than the velocity gradient term for the Reynolds number and the Knudsen number in Case 2A or Case 2B; and for the temperature boundary condition, $T' = 1 + \epsilon T'_2$ is used.

Together with the velocity slip boundary condition, the above equations yield the following results that are consistent with those obtained by Arkilic *et al.* previously:

$$u_1(x', y') = -\frac{\epsilon Re}{8\gamma Ma^2}\left(\frac{\mathrm{d}p_1}{\mathrm{d}x'}\right)(1 - 4y'^2 + 4\Theta_u Kn(x')), \tag{4.4}$$

$$v_2(x', y') = \frac{\epsilon Re}{8\gamma Ma^2 p_1}\left[\frac{1}{2}\frac{\mathrm{d}^2 p_1^2}{\mathrm{d}x'^2}\left(y' - \frac{4}{3}y'^3\right) + 4y'\Theta_u \frac{\mathrm{d}^2 p_1}{\mathrm{d}x'^2} Kn_o\right], \tag{4.5}$$

$$p_1(x') = -6\Theta_u Kn_o + \sqrt{(6\Theta_u Kn_o)^2 + (1 + 12\Theta_u Kn_o)x' + (P^2 + 12\Theta_u Kn_o P)(1 - x')}, \tag{4.6}$$

where Kn_o is the Knudsen number at the channel exit. The derivation of $v_2(x', y')$ utilizes the continuity equation and the condition $p_1 = \rho_1$, obtained by expanding the state equation $p_1 + \epsilon p_2 = (\rho_1 + \epsilon \rho_2)(1 + \epsilon T_2)$. Hence, the isothermal assumption is relaxed.

For Case 2A, the three terms in (4.2) have the same order of magnitude; for Case 2B, the leading term in (4.2) is the one on the left-hand side. For both cases (4.2) is solvable with the temperature jump conditions. The temperature solutions for both

cases share the same form:

$$T_2(x', y') = A(x')B(y') + D(x'), \tag{4.7}$$

where

$$A(x') = \frac{\gamma - 1}{8\gamma^2}\frac{PrRe^2\epsilon}{Ma^2}\left(\frac{\mathrm{d}p_1}{\mathrm{d}x'}\right)^2, \quad B(y') = \left(\frac{1}{2} + 2Kn(x')\Theta_u\right)y'^2 - y'^4,$$
$$D(x') = -\frac{4\gamma A(x')\Theta_T\Theta_u Kn^2(x')}{Pr(\gamma+1)} - A(x')\left[\frac{1}{2}Kn(x')\Theta_u + \frac{1}{16}\right] + \frac{T_w - 1}{\epsilon}.$$

The velocity slip and the temperature jump along the wall can be explicitly obtained from (4.4) and (4.7), on $y' = 1/2$:

$$u_1(x') = -\frac{\epsilon Re\Theta_u}{2\gamma Ma^2}\frac{\mathrm{d}p_1}{\mathrm{d}x'}\frac{Kn_o}{p(x')}, T'_{jump}(x') = \frac{(1-\gamma)Re^2\epsilon^2}{2\gamma(\gamma+1)}\left(\frac{\mathrm{d}p_1}{\mathrm{d}x'}\right)^2\frac{\Theta_u\Theta_T Kn_o^2}{p_1^2(x')}.$$

The non-dimensional and dimensional mass flow rates are

$$Q' = \frac{\epsilon Re}{24\gamma Ma^2}[P-1][P+1+12\Theta_u Kn_o], \quad Q \sim O(\mu Re(P+1+12\Theta_u Kn_o)). \tag{4.8}$$

5. Asymptotic solutions for flows in a microtube

For the gas flows in a microtube with a circular cross-section, with the Mach and Reynolds numbers listed in Case 2A and Case 2B, all the processes described in the previous sections are applicable, and the simplified equations and results are

$$\frac{\epsilon Re}{\gamma Ma^2}\frac{\mathrm{d}p_1}{\mathrm{d}z'} = \frac{\partial}{r'\partial r}\left(r'\frac{\partial u'}{\partial r'}\right), \quad \frac{\partial(p_1u_1)}{\partial z'} + \frac{\partial(p_1r'v_2)}{r'\partial r'} = 0, \tag{5.1}$$

$$\frac{1}{RePr}\frac{\partial}{r'\partial r'}\left(r'\frac{\partial T_2'}{\partial r'}\right) = -\frac{\gamma-1}{\gamma}u_1\frac{\mathrm{d}p_1}{\mathrm{d}z'} - \frac{(\gamma-1)Ma^2}{\epsilon Re}\left(\frac{\partial u_1}{\partial r'}\right)^2; \tag{5.2}$$

and the velocity slip and temperature conditions are, on $r' = 1/2$,

$$u'_w = \Theta_u Kn(z')\left(\frac{\partial u'}{\partial n'}\right)_w, \quad 1 + \epsilon T_2 - T'_w = \Theta_T\frac{2\gamma}{Pr(\gamma+1)}\epsilon Kn(z')\left(\frac{\partial T_2}{\partial n'}\right)_w. \tag{5.3}$$

The corresponding solutions are

$$u_1(z', r') = -\frac{\epsilon Re}{16\gamma Ma^2}\frac{\mathrm{d}p_1}{\mathrm{d}z'}\left(1 - 4r'^2 + 4\Theta_u Kn(z')\right), \tag{5.4}$$

$$v_2(z', r') = \frac{\epsilon Re}{8\gamma Ma^2 p_1}\left[\frac{\mathrm{d}^2p_1^2}{\mathrm{d}z'^2}\left(\frac{r'}{8} - \frac{1}{4}r'^3\right) + r'\Theta_u\frac{\mathrm{d}^2p_1}{\mathrm{d}z'^2}Kn_o\right], \tag{5.5}$$

$$p_1(z') = -8\Theta_u Kn_o + \sqrt{(8\Theta_u Kn_o)^2 + (1+16\Theta_u Kn_o)z' + [P^2 + 16P\Theta_u Kn_o](1-z')}, \tag{5.6}$$

$$T_2(z', r') = A(z')B(r') + D(z'), \tag{5.7}$$

where

$$A(z') = \frac{\gamma - 1}{4\gamma^2}\frac{PrRe^2\epsilon}{Ma^2}\left(\frac{\mathrm{d}p_1}{\mathrm{d}z'}\right)^2,\ B(r') = \left(\frac{1}{16} + \frac{1}{4}Kn(z')\Theta_u\right)r'^2 - \frac{1}{8}r'^4,$$

$$D(z') = -\frac{\gamma A(z')\Theta_T\Theta_u Kn^2(z')}{2Pr(\gamma+1)} - A(z')\left[\frac{1}{16}Kn(z')\Theta_u + \frac{1}{128}\right] + \frac{T_w - 1}{\epsilon}.$$

The velocity slip and the temperature jump along the wall explicitly obtained from (5.4) and (5.7) are, on $r' = 1/2$,

$$u_1(z') = -\frac{\Theta_u\epsilon Re}{4\gamma Ma^2}\frac{\mathrm{d}p_1}{\mathrm{d}z'}\frac{Kn_o}{p(z')},\quad T'_{jump}(z') = \frac{(1-\gamma)Re^2\epsilon^2}{8\gamma(\gamma+1)}\left(\frac{\mathrm{d}p_1}{\mathrm{d}x'}\right)^2\frac{\Theta_u\Theta_T Kn_o^2}{p_1^2(z')}.$$

The non-dimensional and dimensional mass flow rates are

$$Q' = \frac{\epsilon Re}{32\gamma Ma^2}[P-1][P+1+16\Theta_u Kn_o],\quad Q \sim O(\mu Re(P+1+16\Theta_u Kn_o)). \quad (5.8)$$

Finally we offer some comments to conclude the analytical work:

(i) The isothermal assumption is replaced by a quasi-isothermal condition, $T' = 1 + \epsilon T_2$, which is critical to obtain the temperature solution. It is valid for flows with a slow speed and small temperature variations, but not applicable to high-speed gas flow in a channel or tube with electric–magnetic field effects.

(ii) The results obtained are asymptotic solutions to the flow in a channel or tube with two specific combinations of the Reynolds and Mach numbers. However, other asymptotic solutions may exist with different combinations of Mach and Reynolds numbers obeying X-momentum equation as well. There may even exist other solutions that are only obtainable by numerical simulations.

(iii) The pressure distribution for gaseous flows in a microtube varies nonlinearly with z'. For non-slip wall boundary conditions with $Kn \to 0$, the pressure distribution in a channel or a tube follows the same equation: $p_1(z') = \sqrt{z' + P^2(1-z')}$, and the U-velocity contours are similar with a difference factor of 2.

(iv) In the literature, some researchers suggest the following simplified energy equation to study the temperature field: $\rho u C_p \partial T/\partial z = \frac{1}{r}(\partial/\partial r)(kr\partial T/\partial r) + \mu(\partial u/\partial r)^2$. This equation is inappropriate for the pressure-driven gas flow in a microchannel or a tube with a quasi-isothermal assumption, because it improperly neglects the term $\mathrm{d}p/\mathrm{d}z$ which is one order larger than $\mathrm{d}T/\mathrm{d}z = \epsilon\mathrm{d}T_2/\mathrm{d}z$.

(v) Some researchers use a second-order slip model for the wall boundary conditions, $u_s = -A_1(Kn/\rho)(\partial u/\partial y) - A_2(Kn^2/\rho^2)(\partial^2 u/\partial y^2)$, see Qin *et al.* (2007). For this treatment, an extra term with temperature gradient should be included, since it is not smaller than the second term in the expression.

6. Numerical results

To validate the asymptotic solutions for the compressible flows in a microchannel or a microtube, we simulate the following two test cases, where the first has large temperature variations and the second illustrates large temperature gradients even with very small temperature variations:

Case A: Microchannel flow, $L = 20\,\mu\mathrm{m}$, H (or D) $= 1.2\,\mu\mathrm{m}$, $p_i = 3.0 \times 10^5$ Pa;

Case B: Microtube flow, $L = 15\,\mu\mathrm{m}$, H (or D) $= 0.53\,\mu\mathrm{m}$, $p_i = 2.5 \times 10^5$ Pa.

For both cases, $p_o = 1.0 \times 10^5$ Pa, $T_w = 300$ K, and the accommodation coefficients $\sigma_u = \sigma_T = 0.85$. The working gas is oxygen having a Prandtl number $Pr = 0.72$ and a specific heat ratio $\gamma = 1.4$.

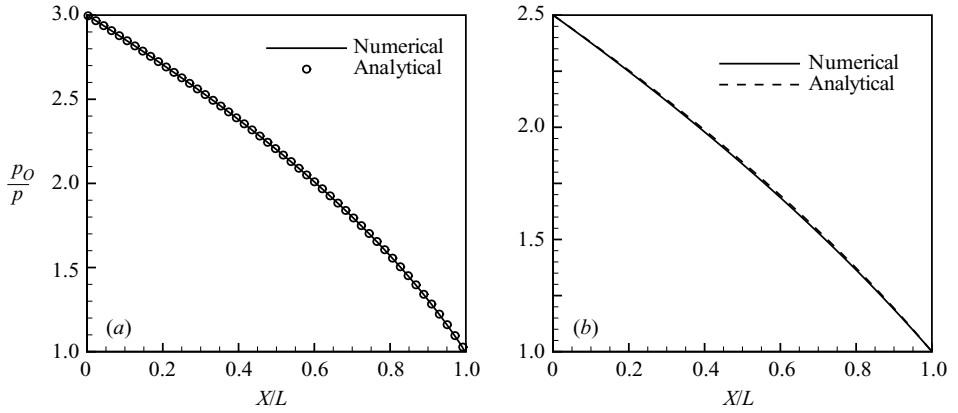

FIGURE 1. Comparison of centreline pressure profiles: (*a*) microchannel, (*b*) microtube.

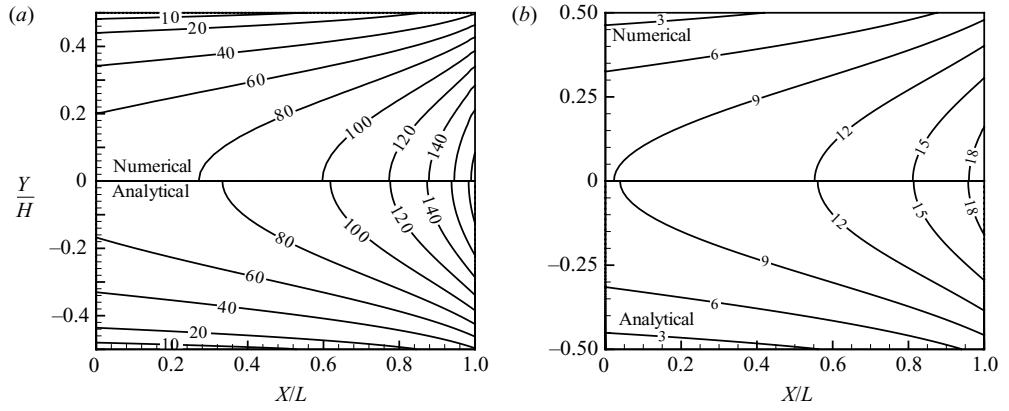

FIGURE 2. U-Contours ($\mathrm{m\,s^{-1}}$) from analytical and numerical simulation: (*a*) microchannel, (*b*) microtube.

Figures 1(*a*) and 1(*b*) show the analytical and numerical results for the pressure profiles along the centreline for the microchannel and microtube respectively. The analytical and numerical results fit very well, and the nonlinear effects are obvious.

Figures 2(*a*) and 2(*b*) show the U-velocity contours that show clear velocity slip along the wall. Again, very good agreement between the analytical and numerical simulation results are obtained. The validity of the analytical results for the pressure distribution in a microchannel has been tested by many other researchers. Hence these two simulation results show that our solution of the compressible Navier–Stokes equation is reliable. Figures 3(*a*) and 3(*b*) show the contours for the velocity component normal to the flow direction. The V-velocity values are zero on the wall and centreline. The microtube flow has smaller velocities than the microchannel. Generally, the numerical and the analytical results match very well.

Figures 4(*a*) and 4(*b*) show the temperature contours. For the microchannel flow, the temperature distributions have larger variations than for the microtube flow. It is clear that the temperature field formula is correct. Two factors account for

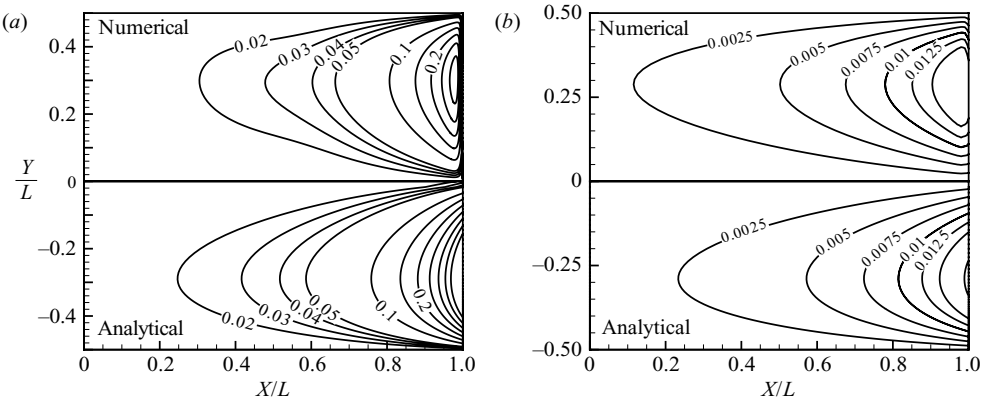

FIGURE 3. V-Contours ($\mathrm{m\,s^{-1}}$) from analytical and numerical simulation: (a) microchannel, (b) microtube.

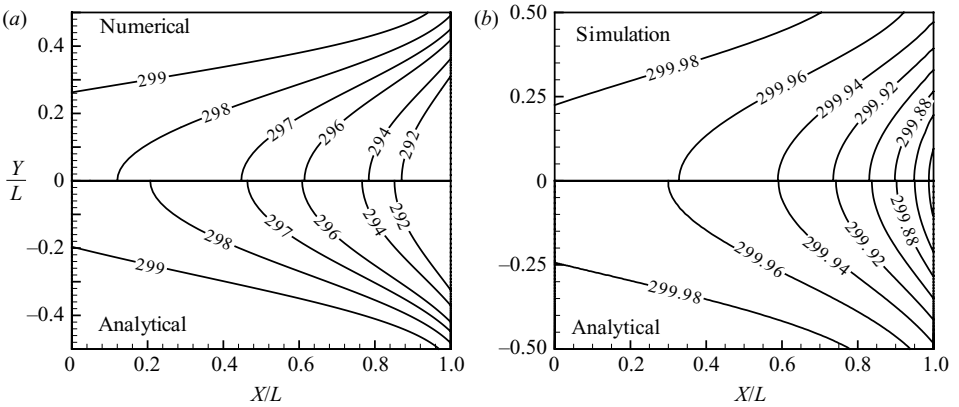

FIGURE 4. Temperature contours (K) from analytical and numerical simulation: (a) microchannel, (b) microtube.

the discrepancies between the numerical and analytical temperature results: (a) the analytical expression contains a term $(\mathrm{d}p/\mathrm{d}x)^2$, resulting in a large difference even with a small difference in $p(x')$; (b) numerically, the heating effects at the channel entrance can be large, but the analytical results do not have any entrance effects.

Figure 5(a) shows the density contours for the microchannel flow. The analytical results are computed with $\rho(x', y') = p(x')/(1 + \epsilon T_2(x', y'))$. If the isothermal assumption were followed, the density field contours would be straight, but this plot clearly shows that the density contours are not straight when considering the temperature field. Xu & Li (2004) also has a similar plot of density contours. For the microtube flows, the density contours are straight and are not included here.

Figure 5(b) shows the analytical velocity slip and the temperature gradients along the channel and the tube wall: the magnitude of $\mathrm{d}T/\mathrm{d}n$ is significant. Even for the microtube case, the gradient is large due to the small dimension. Hence, it is important to study the temperature field for microflows.

We also perform several simulations to validate the fundamental Reynolds–Mach number relation, and the mass flow rate relation, for a microchannel. Two series of simulations are performed where the pressure ratio varies from 1.8 to 3.0, and

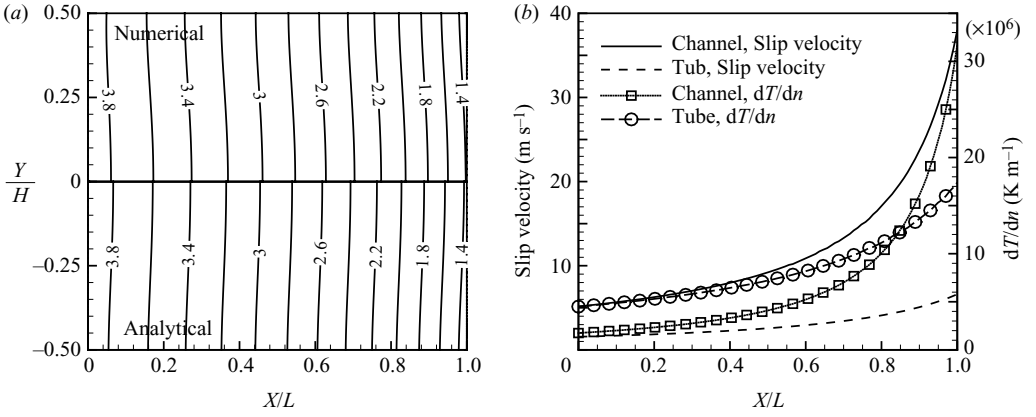

FIGURE 5. (*a*) Microchannel: Normalized density contours. (*b*) Analytical wall slip velocity and temperature gradients for the microchannel and microtube.

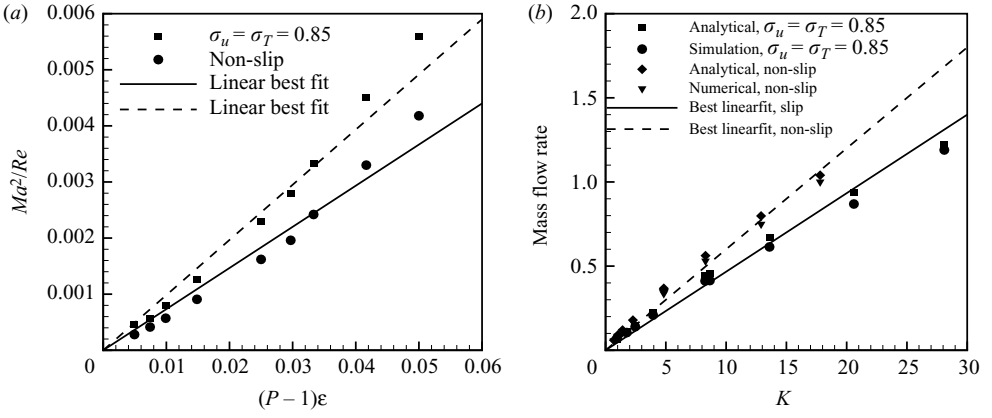

FIGURE 6. Microchannel: (*a*) Relations between Ma^2/Re and $(P-1)\epsilon$ at channel outlets. (*b*) Dimensional mass flow rate vs. K, where $K = Re(P + 1 + 12\Theta_u Kn_o)$ for slip flows and $K = Re(P + 1)$ for non-slip flows.

the channel length varies from 36 μm to 216 μm, while the channel height is fixed at $H = 0.53$ μm. Both slip and non-slip wall boundary conditions are used. The simulation results indicate that they belong to either Case 2A or Case 2B. Figure 6(*a*) shows the relation between the pressure ratios, P, the channel dimension ratio, ϵ, and the Reynolds/Mach numbers at the channel outlets. Near-linear relations are obtained as predicted by our analysis in § 3. Each symbol represents one simulation for a microchannel with a different combination of parameters by varying the channel length, pressure or wall boundary conditions. Two straight lines are added to aid the comparison. Figure 6(*b*) shows the relation between the mass flow rate and $Re(P + 1 + 12\Theta_u Kn_o)$ for the slip flow situation or $Re(P + 1)$ for the non-slip flow situation.

7. Conclusion

In summary, we have performed an order analysis for the outlet Mach and Reynolds numbers, and obtained the temperature field using a quasi-isothermal assumption considering two groups of parameters. The work is based on physical assumptions and mathematic analysis. It naturally extended Arkilic *et al.*'s analytical original work on compressible gas flow in a microchannel. Without the limitation imposed by the isothermal assumption, the results from this study are applicable to microchannel/tubes with temperature variation. The microchannels or microtubes can be very long or very short; the only requirement is that the pressure drop term balances with the viscous term when the convection term is small, or they belong to Case 2 as discussed in § 3.

REFERENCES

Arkilic, E. B., Schmidt, M. A. & Breuer, K. S. 1997 Gaseous slip flow in long microchannels. *J. Micro. Electro. Mech. Sys.* **6**, 167–178.

Arkilic, E. B., Schmidt, M. A. & Breuer, K. S. 2001 Slip flows and tangential momentum accomdation in micromachined channels. *J. Fluid Mech.* **437**, 29–43.

van den Berg, H. R., ten Seldam, C. A. & van der Guli, P. S. 1993 Compressible laminar flow in a capillary. *J. Fluid Mech.* **246**, 1–20.

Cai, C., Boyd, I. D, Fan, J. & Candler, G. V. 2000 Direct simulation methods for low-speed microchannel flows. *J. Thermophys. Heat Tranfser* **14**, 368–378.

Chen, X. 1996 *GasKinetics and Its Applications in Heat Transfer and Flow*. TsingHua University Press, Beijing.

Harley, J. C. & Huang, Y. H. 1995 Gas flow in micro-channels. *J. Fluid Mech.* **284**, 257–274.

Hetstroni, G., Mosyak, A., Pogrebnyak, E. & Yarin, L.P. 2005 Heat transfer in micro-channels: comparison of experiments with theory and numerical results. *Intl J. Heat Mass Transfer* **48**, 5580–5601.

Ho, C. M. & Tai, Y. C. 1998 Micro-electro-mechanical-systems(mems) and fluid flows. *Annu. Rev. Fluid Mech.* **30**, 579–612.

Kedzierski, M. A. 2003 Microchannel heat transfer, pressure drop and macro prediction methods. *2nd Intl Conf. on Heat Transfer, Fluid Mechanics and Thermodynamics* pp. 1057–1063. University of Pretoria.

Pong, K. C., Ho, C. M. & Liu, J. Q. 1994 Nonlinear pressure distribution in uniform microchannels. In *Application of Microfabrication to Fluid Mechanics, ASME Winter Annual Meeting. Chicago.* pp. 51–56.

Prud'homme, R. K., Champman, T. W. & Brown, J. R. 1986 Laminar compressible flow in a tube. *Appl. Sci. Res.* **43**, 67–74.

Qin, F. H., Sun, D. J. & Yin, X. Y. 2007 Perturbation analysis gas flow in a straight microchannel. *Phys. Fluids* **19**, 027103.

Shen, C., Fan, J. & Xie, C. 2003 Statistical simulation of rarefied gas flows in micro-channels. *J. Comput. Phys.* **189**, 512.

Wang, M. & Li, Z. 2004 Micro- and nanoscale non-ideal gas poiseuille flows in a consistent boltzmann algorithm model. *J. MicroMech. Microengng* **14**, 1057–1063.

Xu, K. & Li, Z. 2004 Microchannel flow in the slip regime: Gas-kinetic bgk-burnett solutions. *J. Fluid Mech.* **513**, 87–110.

Zheng, Y., Garcia, A. L. & Alder, B. J. 2000 Comparison of kinetic theory and hydrodynamics for Poiseuille flow. *J. Statist. Phys.* **109**, 368–378.

Zohar, Y. L., Li, S. Y. K., Lee, W. Y., Jiang, L. & Tong, P. 2004 Subsonic gas flow in a straight and uniform microchannel. *J. Fluid Mech.* **472**, 125–151.